Nanoscale

Accepted Manuscript

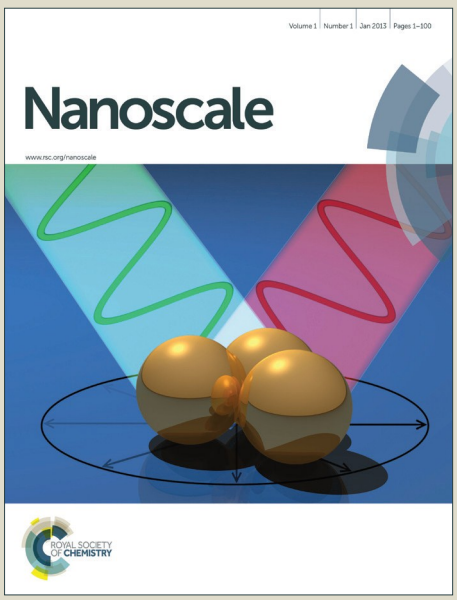

ROYAL SOCIETY OF CHEMISTRY

www.rsc.org/nanoscale

NR-ART-06-2015-003598

Nanoscale-alumina induces oxidative stress and accelerates amyloid beta (Aβ) production in ICR female mice

Shahid Ali Shah PhD, Gwang Ho Yoon MS, Ashfaq Ahmad PhD, Faheem Ullah MS, Faizul Amin PhD and Myeong Ok Kim*

Department of Biology and Applied Life Science, College of Natural Sciences, Gyeongsang National University, Jinju, 660-701, Republic of Korea

* Corresponding author

Myeong Ok Kim, Prof. Ph.D,

Head of Neuroscience Pioneer Research Centre,

Department of Biology and Applied Life Science, College of Natural Sciences,

Gyeongsang National University, Jinju, 660-701, South Korea

Tel.: +82-55-772-1345

Fax: +82-55-772-1349

E-mail: mokim@gsnu.ac.kr

Abstract

The adverse effects of nanoscale-alumina (Al_2O_3-NPs) have been previously demonstrated in both *in vitro* and *in vivo* studies, whereas little is known about its mechanism of neurotoxicity. It is the goal of this research to determine the toxic effects of nano-alumina on human neuroblastoma SH-SY5Y and mouse hippocampal HT22 cells *in vitro* and on ICR female mice *in vivo*. Nano-alumina displayed toxic effects on SH-SY5Y cells lines in three different concentrations also increased aluminium abundance and induced oxidative stress in HT22 cells. Nano-alumina peripherally administered to ICR female mice for three weeks increased brain aluminium and ROS production, disturbing brain energy homeostasis, and led to the impairment of hippocampal dependent memory. Most importantly, these nano-particles induced Alzheimer disease (AD) neuropathology by enhancing the amyloidogenic pathway of Amyloid Beta (Aβ) production, aggregation and implied the progression of neurodegeneration in the cortex and hippocampus of these mice. In conclusion, these data demonstrate that nano-alumina is toxic to both cells and female mice and that prolonged exposure may heighten the chances of developing a neurodegenerative disease, such as AD.

Key words; Nano-alumina, ICR mice, Alzheimer disease, ROS, phospho-tau, SH-SY5Y cells

Introduction

The use of engineered nanoparticles has been increased because of their applications in various fields, such as electronics, biomedical applications, pharmaceuticals, cosmetics, energy applications, and materials, during the last 2 decades[1] and because their toxic side effects are also increasing daily. Recently, various investigators strived to elucidate the deleterious effects of these engineered nanoparticles[2, 3]. Some of these engineered nanoparticles like Ag, TiO_2 and ZnO exists in the environment, drinking water and in various consumer products has been reported to induce inflammation, oxidative stress and cytotoxicity[4-6]. Similarly, the usage of aluminium (Al) and its various nanosized compounds, such as oxides and hydroxides, as nanoparticles have become popular in many applied fields, while on the other hand, due to the neurotoxic nature of aluminium, it has been reported to be associated with several neurodegenerative diseases, especially Alzheimer's disease[7]. Nanosized-alumina has been tested in several rodent animal models where it impaired memory[8], activated microglial cells[9] and also induced autophagy[10]. Regardless of the route of administration of the nano-alumina in animals, these particles can cross the blood brain barrier, (BBB) reach the brain, and produce reactive oxygen species (ROS), causing inflammation and inducing neurotoxicity.

Alzheimer's disease (AD) is characterized by extracellular amyloid deposits, intracellular neurofibrillary tangles, cholinergic deficits, synaptic loss, inflammation and extensive oxidative stress[11]. A growing body of evidence suggests that oxidative stress is involved in the pathophysiology of several neurodegenerative diseases[12, 13], and most importantly, this is believed to be one of the earliest pathological changes in AD[14-16]. Previous work revealed a strong link between aluminium neurotoxicity and AD pathogenesis, such as amyloid-β and hyper-phosphorylated tau-protein accumulation and aggregation as well as forming senile

plaques and neurofibrillary tangles (NFT), respectively[17, 18]. Aluminium can cross the BBB and accumulate in different brain regions, including the cortex and hippocampus, and induce oxidative stress by causing damage to membrane lipids, proteins and the antioxidative enzyme defence system[19-23].

The purpose of this study was to test, for the first time, the adverse effects of nano-alumina on SH-SY5Y and HT22 cells line *in vitro* and simultaneously evaluate the hazardous consequences and cognitive impairment after peripheral administration of these nanoparticles to female ICR mice.

Material & Methods

Chemicals

Nanoscale-alumina (Al_2O_3-NPs) (30-60nm) (Product Number: 642991) Morin hydrate (3, 5, 7, 29, 49-Pentahydroxyflavone) Rhodamine-123 (Product Number: R8004) and Coumarin-6 (Product Number: 442631) were purchased from Sigma Aldrich.

Size and shape determination of nano-alumina

The size and shape of nano-alumina was analysed through Transmission Electron Microscopy (TEM).

Mice Strain and nano alumina treatment

ICR (Institute of Cancer Research) female mice (10 weeks of age) used in the present study were purchased from Sam Tako Inc., Korea. Nano-alumina was administered at 50 mg/kg intraperitoneally (i.p), [9] two times a week for three weeks. Both treated and untreated animals were sacrificed three weeks after nano alumina administration. A great care was taken while

handling the animals. All of the experimental procedures were approved (Approval ID: 125) by the local animal ethics committee (IACUC) of the Division of Applied Life Sciences, Department of Biology Gyeongsang National University South Korea.

Cell Cultures

The following two types of cell cultures were used.

1) Mouse hippocampal HT22 neuronal cells

2) Human Neuroblastoma SH-SY5Y neuronal cells

HT22 (a generous gift from Prof. Koh (Gyeongsang National University) and SH-SY5Y neuronal cells were purchased from KOREAN CELL LINE BANK, Seoul, Korea (KCLB). Both (HT22 and SH-SY5Y) neuronal cells were cultured in DMEM (Dulbecco's modified Eagle medium), containing high D-glucose, 10 % FBS and 1 % antibiotics (penicillin-streptomycin) at 37°C in humidified air containing 5 % CO_2. For performing different assays, the cells were plated in 96-well plates at a required density of at least 70% confluence.

Conjugation of rhodamine-123/Coumarin-6 to nano-alumina and Cellular uptake

For fluorescence-labeled nano-alumina formulation, we used a previously described method with some modifications to conjugate rhodamine-123/coumarin-6 to nano-alumina[24]. Briefly, 5 mg of rhodamine-123/coumarin-6 was dissolved in 25 ml of acetone, and added to 100 ml of nano-alumina under stirring. This mixture was then further stirred for 3 h at 60 °C and then cooled to room temperature. The solution was then centrifuged at 4000 rpm to remove unattached dye. This procedure was repeated three times to ensure that no free dye molecules remained in the final conjugate.

The uptakes of rhodamine-123/coumarin-6 conjugated nano-alumina were studied in mouse bEnd3 cell line which served as an *in vitro* blood brain barrier (BBB) model (ATCC, USA) and human neuroblastoma SH-SY5Y cells, using confocal microscopy (Fluoview FV 1000, Olympus, Japan). Freshly prepared rhodamine-123/coumarin-6 conjugated nano-alumina suspension at concentration of 0.1 mg/ml was mixed with cell culture medium and added to the cells pre-cultured in 4-well cover glass chambers and incubated for 24 h. Following incubation, the cells were washed three times with PBS and were fixed with 4% NBP and rinsed with PBS and incubated with DAPI for 5 min. The slides were then rinsed with PBS and glass cover slips were mounted on glass slides with mounting medium, and fluorescent images were captured with confocal microscope.

Incubation with nanoparticles

After 24 h of incubation for HT22 cells and 48 h of incubation for SH-SY5Y cells under the above-mentioned conditions, the culture medium was removed and replaced with medium containing nano-alumina at three different concentrations (100, 125 and 150 μg/ml). Incubation was continued for another 12 and 24 h. Control cells were cultured under similar conditions in culture medium without added nanoparticles.

ApoTox-Glo^{TM} Triplex assay *in vitro*

To estimate the levels of cell viability, cytotoxicity and caspase-3 activity in a 96-well assay plate, we performed the ApoTox-Glo^{TM} Triplex assay (Promega Corporation 2800 Woods Hollow Road Madison, WI53711 USA) previously described by[25] , with a slight alteration. After plating human neuroblastoma SH-SY5Y cells (2 x 10^4 cells/well) in 96-well plates as described above, they were treated with three different concentrations (100, 125 and 150 μg/ml) of Al_2O_3-NPs. The control cells remained untreated. After 24 h of incubation with Al_2O_3-NPs, cell

viability (wavelength $400_{Ex}/505_{Em}$), cytotoxicity (wavelength $485_{Ex}/520_{Em}$) and caspase-3/7 activation were measured according to the manufacturer's instructions (ApoTox-Glo^{TM} Triplex Assay, Promega).

Oxidative stress (ROS) detection.

The method described[26], for ROS detection was followed. Briefly, HT22 and SH-SY5Y neuronal cells were cultured in 96-well plates. After 24 and 48 h respectively, cells were incubated with fresh medium containing three different concentrations (100, 125 and 150 μg/ml) of nano-alumina for 6 h, followed by the addition of a 600 μM solution of DCFDA (2′,7′-dichloroflourescein diacetate) dissolved in DMSO/PBS to each well; cells were then incubated for 30 min. The plates were read in ApoTox-Glo^{TM} (Promega) at 488/530 nm.

Morris water maze (MWM) Test

Mice were assessed for spatial reference memory in the Morris water maze (MWM) [27]. The MWM apparatus consisted of circular water tank (100 cm dia. x 40 cm H), containing water (22 ± 1°C, 26 cm H) that had been rendered opaque by the addition of nontoxic water-soluble white ink. A platform (5 cm dia. x 25 cm H) was submerged approximately 1 cm below the water surface in the middle of one quadrant. Experimental tools were located in behaviour test room to acclimatize the mice and prevent disturbing factors during training and testing. The mice were first trained for 3 consecutive days (4 trials per day). Latency to escape from the water maze by finding the submerged escape platform was calculated over 60 sec. If a mouse was unable to find the submerged platform in 60 sec, it was gently guided to the platform and allowed to stay on platform for 10 sec. After 3 weeks of nano-alumina treatment, the escape latency of the mice was recorded for 4 days. Finally, the probe test without the submerged platform was conducted and the time spent in platform quadrant was recorded.

Western blotting

Western blots were performed as we reported earlier[28]. The brain cortical and hippocampal sections were carefully separated from both treated and untreated female mice and homogenized. The protein concentration in the brain tissue homogenates was estimated by the Bio-Rad protein assay (Bio-Rad Laboratories, CA, and USA). Throughout the entire study, equal amounts (20 μg) of protein were subjected to SDS-PAGE on 4-12% Bolt ™ Mini Gels (Novex, Life technologies) and transferred to a PVDF membrane. Non-specific binding was reduced by blocking the membrane in 5 % skim milk and incubated with primary antibodies at 4^0C overnight. The primary antibodies used were: anti-β-actin, anti-PSD95, anti-caspase-3, anti-AMPK, anti-p-AMPK Thr^{172} (Cell Signalling Technology, Inc.), anti-amyloid C-terminus, anti-BACE-1, anti-total tau anti-phospho-tau (Ser^{413}), anti-PARP-1 and anti-Synaptophysin (Santa Cruz Biotechnology, Santa Cruz, CA, USA) and anti-APP (Millipore technologies, respectively). After washing with 1X TBST and incubating with horseradish peroxidase-conjugated secondary antibodies, protein bands were detected using ECL reagents according to the manufacturer's instructions (Amersham Pharmacia Biotech, Uppsala, Sweden). X-ray films were scanned, and band intensities were analysed by densitometry using Sigma Gel software (SPSS, Chicago, IL, USA).

Brain tissue collection for morphological assessment

Mouse brain tissue was fixed by transcardial perfusion with 4% ice-cold paraformaldehyde. Post-fixation of the brains was continued for the next 72 h in 4 % paraformaldehyde and then in 20 % sucrose for 72 h at 4^0C. An Optimal Cutting Temperature (OCT) compound (A.O., USA) was used for mounting the brains followed by freezing them in liquid nitrogen and sectioning (14

μm) in the coronal plane with a CM 3050C cryostat (Leica, Germany). The tissue sections were mounted on Probe On Plus charged slides (Fisher, USA).

Morin Staining

To detect the aluminium accumulation in HT22 cells and in the brain of mice treated with nano-alumina, we performed Morin staining (3, 5, 7, 29, 49-Pentahydroxyflavone) as previously described[29]. The Morin solution was made by mixing 0.2% Morin reagent in 85% ethanol containing 0.5% glacial acetic acid. Slides containing HT22 cells and mouse brain tissues were immersed in a 1% aqueous solution of hydrochloric acid for 10 min, followed by washing and immersion in the Morin solution for 10 min and DAPI counterstaining for 5 min. Glass cover slips were mounted on slides with mounting medium, and images were taken using confocal laser scanning microscope (FV 1000, Olympus, Japan).

Fluoro-Jade B staining

Procedure for Fluoro-Jade B (FJB) staining was followed as we reported earlier[30]. Overnight air-dried brain tissue slides were immersed in a solution of 1% sodium hydroxide and 80% ethanol for 5 min, followed by immersion in 70% ethanol for 2 min, distilled water for 2 min, and 0.06% potassium permanganate solution for 10 min and a rinse with distilled water. Subsequently, the slides were immersed in a 0.01% FJB solution for 20 min, rinsed with distilled water and were allowed to dry for 10 min and immersed in DAPI solution for 10 min. Glass cover slips were mounted on the slides using mounting medium. A FITC filter on a confocal laser scanning microscope (FV 1000, Olympus, Japan) was used for capturing images.

Immunofluorescence analysis

An immunofluorescence study was conducted following the procedure recently reported [26], with slight modifications. In the beginning, slides containing tissue sections were washed twice for 15 min in 0.01 M PBS. Then, the tissues were incubated with proteinase K at 37°C for 5 min followed by incubation for 1 h in blocking solution (5% normal goat serum, 0.3% Triton X-100, PBS). After the blocking step, the primary antibodies (anti-p-AMPK, Aβ (6E10, BioLegends) and anti-8-oxoguanine (Millipore) were applied to the slide containing cells and the tissues overnight followed by incubation with a secondary FITC/TRITC -conjugated antibody (1:50 dilution in PBS; Santa Cruz) at room temperature for 90 min. Propidium Iodide (PI) staining was performed 5 min before mounting of slides. Prolong Antifade Reagent (Molecular Probe, Eugene, OR, USA) was used to mount the slides. All of the immunostained slides were examined using a confocal laser-scanning microscope (Flouview FV 1000). All of the immunofluorescence signals were analysed by Image J Software (open source software provided by the National Institutes of Health, USA.) and expressed as Integral Optical Density (IOD).

Thioflavin S staining

Amyloid plaques were investigated in the brain sections using Thioflavin S staining. Slides containing brain sections were washed twice in 0.01 M PBS for 10 min, then immersed in a fresh solution of 1 % Thioflavin S for 10 min at room temperature. Sections were then immersed in 70 % ethanol for 5 min, rinsed 2 times in water, counterstained with PI and covered with a cover slip.

Enzyme assays

Both CycLex AMPK kinase (CycLex Co., Nagano, Japan) and $A\beta_{1-42}$ assay (Invitrogen; Camarillo, CA) kits were used to measure the activated AMPK and $A\beta$-$_{1–42}$ levels in both nano-alumina treated and untreated mice brain homogenates according to manufacturer's instructions.

Statistical analysis

The original X-ray films of the western blots were scanned, and their densities analysed by using computer based Sigma Gel System (SPSS Inc.) software. Densities were normalized to the untreated control and all the experimental results *in vitro* repeated in triplicate were expressed as the mean ± SEM. Morphological images were analysed for their IOD (Integrated Densities) with Image J software. Prism 5 (Graph Pad Software, Inc., San Diego, California) was used for one way analysis of variance (ANOVA) followed by Student's t-test. Data were considered significant at $p< 0.05$, 0.01 and 0.001.

Results

Characteristics of nano-alumina

The nano-alumina particle size was analyzed by transmission electron microscope (TEM). These nano particles are mixture of various sizes. The TEM images shown in Fig. 1 reveal that these particles were of oval shaped and of various sizes ranging from 30-60 nm.

The toxic effects of nano-alumina *in vitro*

First, we analysed the toxic effects of nano-alumina *in vitro*. To investigate whether nano-alumina in three concentrations (100, 125 and 150 μg/ml) was toxic to human neuroblastoma SH-SY5Y neuronal cells *in vitro,* the Apo-Tox Glo^{TM} Triplex assay was performed. This assay

consisted of three steps including 1). Cell viability, 2). Cytotoxicity and 3). Apoptosis (apoptotic marker caspase-3/7). The cells were exposed for 24 h to 100, 125 and 150 μg/ml of nano-alumina, and all concentrations caused a significant reduction in the number of viable SH-SY5Y cells, induced cell toxicity and increased the activation of caspase-3/7 significantly compared to the control (Fig. 2A).

To further analyse the nano-alumina toxicity regarding oxidative stress, 100, 125 and 150 μg/ml of nano-alumina were investigated for producing reactive oxygen species (ROS). The results indicated that in contrast to untreated control cells, the three concentrations of nano-alumina significantly produced ROS in both SH-SY5Y and HT22 cells after exposure for 6 h (Fig. 2B).

Cellular uptake of nano-alumina by cells

The uptakes of nano-alumina by mouse bEnd3 and SH-SY5Y cells were conducted by using confocal microscopic analyses. We investigated the intracellular retention, of rhodamine-123-conjugated nano-alumina in cultured mouse bEnd3 cells and coumarin-6-conjugated nano-alumina in cultured SH-SY5Y cells. Our results showed that both rhodamine-conjugated nano-alumina and coumarin-conjugated nano-alumina were efficiently internalized by mouse bEnd3 cells (Fig. 2C) and SH-SY5Y (Fig. 2D). These results indicate that nano-alumina can cross BBB and reach the brain and hence inducing its toxic effects to neurons after 24 h.

Nano-alumina increased aluminium abundance and induced oxidative stress both *in vitro* and *in vivo*

To analyse whether HT22 cells can take up nano-alumina and increase their aluminium level, Morin staining was performed. Exposure of HT22 cells to nano-alumina caused an increased uptake of nano-alumina, which ultimately increased the aluminium abundance as evident from

Fig. 2C. Furthermore, to assess oxidative stress induced by nano-alumina in HT22 cells, 8-Oxo-guanine (8-OxoG) staining was performed using an anti-8-OxoG monoclonal antibody. The immunofluorescence images show that nano-alumina induced oxidative stress and produced a significantly high number of ROS in the treated cells in contrast to untreated HT22 cells (Fig. 2D).

In the second phase, nano-alumina was peripherally administered for three weeks to ICR female mice and the mouse brain tissue was evaluated for the abundance of aluminium. The results indicate that exogenously administered nano-alumina significantly increased brain aluminium abundance compared to untreated control mice. These immunohistological evaluations for abundance of brain aluminium were conducted in the hippocampal CA1, CA3 and DG and cortical regions of the female mouse brain (Fig. 3A). Similarly, to analyse the extent of oxidative stress induced by nano-alumina, *in vivo* 8-OxoG staining was performed. It was evident from the immunostaining images that nano-alumina induced oxidative stress by increasing 8-OxoG expression in the brains of exposed mice. This trend was mainly observed in different parts of the hippocampus including cornu ammonis 1 and 3 (CA1 and CA3 respectively) and dentate gyrus (DG) and the cortical regions in treated mice, while no or only few 8-OxoG appearances were seen in the hippocampus and cortical regions in the untreated control mice (Fig. 3B).

The effects of nano-alumina on behaviour and memory in mice

After analysing the toxic effects of nano-alumina *in vitro* and brain aluminium abundance *in vivo,* we investigated the adverse effects of these nano-particles on behaviour and memory in female ICR mice using the Morris Water Maze (MWM) task. We analysed the escape latency time of these mice to measure spatial learning and memory before and after the injection of nano-alumina. As shown in Fig. 4A both treated and untreated mice had a similar escape latency

time in finding the submerged platform, and there were no significant differences before nano-alumina administration. However, after nano-alumina exposure for three weeks, the mice showed significant memory impairment and a higher escape latency compared to a littermate control assessed on the first day. Furthermore, their escape latency in finding the submerged platform gradually decreased on day two and three, respectively, because there was no treatment during those days, but it was still higher than in untreated mice. Interestingly, when nano-alumina was injected on day four, the escape latency once again rose sharply compared to the untreated control, indicating that nano-alumina were involved in spatial memory impairment (Fig. 4B).

After escape latency analysis probe test was performed by removing the platform. In the probe test, the time spent in the target quadrant by nano-alumina treated mice was significantly lower as compared to untreated control, indicating that these nanoparticles treatment partially impaired spatial learning and memory deficit in ICR female mice (Fig. 4C).

Nano-alumina induced Aβ production via amyloidogenic pathway in mice

We extended our study further to investigate Aβ production via the amyloidogenic pathway as a consequence of nano-alumina treatment in mice. The western blot results show that the administration nanoparticles to mice enhanced the amyloidogenic pathway of Aβ production. Nano-alumina upregulated the expression of the amyloid precursor protein (APP) and β-secretase BACE1 (beta-site amyloid precursor protein cleaving enzyme 1) activity, which significantly increased the generation of Aβ in treated mice compared to the untreated control. Moreover, it also caused downregulation of the α-secratase enzyme sAPP-α, which is responsible for the generation of non-toxic Aβ peptides through a non-amyloidogenic pathway (Fig. 4D). The levels of soluble $A\beta_{1-42}$ in the brain homogenates was measured through ELISA method which revealed that nano-alumina significantly increased the production of $A\beta_{1-42}$ (Fig. 4E).

Interestingly, nano-alumina also caused the formation of Aβ aggregation and plaques in the hippocampus and cortical regions of the brain in treated mice, which was investigated immunohistopathologically both via Aβ (6E10) antibody and Thioflavin S staining (Fig. 5A). We also investigated via western blot whether an increase in the Aβ level produced by nano-alumina had any effect on the hyperphosphorylation of microtubule-associated tau at (ser^{413}) and synapse related proteins, including Synaptophysin and post-synapse density protein 95 (PSD 95). These analyses indicated that Aβ induced a significant increase in the expression level of p-tau (while the total tau protein level was unchanged) (Fig. 5C) and downregulated the expression of Synaptophysin and PSD 95 proteins in treated mice compared to the control (Fig. 5D).

Nano-alumina induced AMPK inhibition *in vivo*

The effect of nano-alumina on brain energy metabolism was evaluated in treated and untreated mouse brain homogenates via western blot. These results indicated that nano-alumina reduced the expression of AMPK by inactivating and dephosphorylating it at Thr^{172} in the brain compared to untreated mice, while the total AMPK level remain unchanged (Fig. 6A). Similarly, the AMPK activity was also reduced in the brain homogenates of nano-alumina treated mice analysed through the Cyclex AMPK activity assay method (Fig. 6B). Additionally, the expression of p-AMPK was investigated via immunofluorescence in the hippocampal CA1 and cortical regions of nano alumina treated and untreated mice. These images of immunofluorescence revealed that nano-alumina significantly inhibited the expression of p-AMPK, which supported our western blot results, suggesting that these nanoparticles are involved in the disturbance of brain energy metabolism (Fig. 6C).

Nano-alumina induced neurodegeneration *in vivo*

The toxic effect of administered nano-alumina in inducing neurodegeneration was further examined by analysing the expression of apoptotic markers via western blot. Our results indicated that nano-alumina significantly upregulated the expression of various apoptotic markers, such as cleaved caspase-3 and cleaved PARP-1, in the hippocampus and cortical sections of the mouse brain, as shown in the western blot results in Fig. 7A. However, caspase-3 and PARP-1 were less expressed in untreated mice. Additionally, Flouro Jade B (FJB) staining was performed to investigate the toxicity of administered nano-alumina for inducing neurodegeneration in the hippocampus and cortical regions in mice. Investigation of the cortical and hippocampal CA1, CA3 and DG regions of nano-alumina-treated mice reveals that these nanoparticles induced neuronal cell death, as was evident from the number of positive FJB cells, whereas no such signals were observed in the control mouse brain sections (Fig. 7B).

Discussion

This study demonstrated for first time the deleterious effects of nano-alumina exposure to a human neuroblastoma and mouse neuronal cell line *in vitro* and to a female mouse brain *in vivo*. These findings highlight that nano-alumina are responsible for the production of ROS and are very toxic to both human and mouse neuronal cells.

Here we have demonstrated that the administration of nanosized alumina increased the abundance of metallic aluminium in the mouse brain, which indicated that this might be the initial stage inducing deleterious effects because mounting evidence has suggested that aluminium accumulation has severe toxic manifestations in the central nervous system. We used an ICR mice strain that is widely used in the neurosciences field, especially in the Morris water Maze (MWM). Indeed, earlier report[31] demonstrates that there are sex differences between male

and female mice in this strain, and their results indicate a poor MWM behaviour performance for male mice compared to female mice. Additionally, another report[5] have shown that nanosized alumina induce behaviour impairment in ICR male mice. Additionally, various animal studies have shown that aluminium exposure causes aluminium accumulation in all regions of rat brain following chronic exposure, the maximum amount is seen in hippocampus, which is the site of memory and learning[32, 33]. A similar finding in previous studies also demonstrated that aluminium is responsible for inducing neuropathological, neurobehavioral, neurophysical and neurochemical alterations that ultimately result in memory impairment[34, 35]. Moreover, there is close association between high concentrations of aluminium in drinking water and AD[36], but the exact mechanism is still unexplained. In this study, we demonstrated for the first time that nano-alumina induced AD-like pathology and not only enhanced toxic Aβ production via the amyloidogenic pathway in mice but also its accumulation and aggregation in the form of Aβ plaques. Along with increased Aβ production, nano-alumina caused the upregulation of the hyperphosphorylation of microtubule-associated tau proteins in treated mice, suggesting that p-tau production and accumulation are Aβ-dependent.

The literature indicates that Aβ interacts with signalling molecules that are involved in the hyperphosphorylation of microtubule-associated tau proteins[37, 38]. Hyperphosphorylated tau accumulation causes neurofibrillary tangles (NFT) that are rated to a highly toxic form of soluble tau. The accumulation of these proteins, including Aβ and p-tau, affects normal communications among neurons, causing the synapse disturbance that is an AD hallmark. Apart from senile plaques and neurofibrillary tangles, AD brains also show synaptic dysfunction, activated microglia, gliosis, activation of inflammatory markers, ROS production and neurodegeneration[39]. Consistent with the previous studies, this work has noted that nano-alumina caused reduced

expression of pre- and post-synapse related proteins, including synaptophysin and PSD 95, and affected their communication, inducing synaptic dysfunction in mice. Similarly, our results indicate that nano-alumina exposure induced oxidative stress and produced ROS in cells and in mice, and their accumulation and aggregation in the brain caused some serious CNS disorders, particularly AD. Other studies performed to analyse the toxicity of nano-alumina have demonstrated that these nanomaterials induce oxidative stress and inflammation[40, 10]. In this regard, the work of Li[9], which reported that these nanoparticles induced the activation of the glia in the brain even when peripherally administered, is very important.

Oxidative stress is the hallmark feature of exposure to metals or metallic oxide nanoparticles both *in vitro* and *in vivo*. Various nanosized materials such as Ag, ZnO and TiO_2 when introduced into the cells of different types generate ROS in a[4-6]. Similarly, these authors have also shown that due to the existence of these metals and their oxides nanoparticles in natural environment, drinking water and daily stuff extremely increased their health hazardous effects. Furthermore, they pointed out that ZnO induces oxidative stress and neurodegeneration in p53 dependent manner, while a TiO2 nanomaterial causes endothelial cell leakiness[6, 41]. Other studies conducted have demonstrated that exposure of intestinal cells to SiO2, TiO2 and ZnO results in a high amount of ROS production, inflammation, DNA damage and finally cell death[42, 43]. Interestingly, they were very successful in predicting some of the physico-chemical parameters of engineered nanoparticles and biological responses[44].

A large number of studies have proven that, although aluminium is not a transition metal that accelerates redox reactions[45], it has the ability to induce neurotoxicity through the generation of free radicals[46, 47]. Several studies claimed that aluminium induces malfunctions in mitochondria both *in vivo* and *in vitro*[48], and can impair the antioxidant defence system to potentiate oxidative

stress[49], and damage DNA, which is more susceptible to oxidation. In cells, mitochondria are responsible for the generation of ROS and also are the location of ROS damage to the cell. One of the most important and common consequences of ROS and the index of oxidative damage, is the production of 8- Oxo-guanosine (8-OxoG)[50]. Additionally, overproduction of superoxide radicals within the mitochondria will cause the accumulation of the oxidized product 8-OxoG in their DNA[51]. Indeed the work of Kumar[52] reveals that aluminium lactate and $AlCl_3$ can induce oxidative stress in the hippocampus and the cortex of exposed rats and mice.

As the powerhouse of the cells, the mitochondria play a major role in energy metabolism, and it has been previously reported that aluminium exposure disrupts the normal functioning of mitochondria in neuronal cells. In this study, nanosized alumina disrupted energy metabolism in mice by deactivating and dephosphorylating AMPK at Thr^{172}. These findings are similar to an earlier study that showed a decrease in ATP production in human hepatocytes after treatment with aluminium[53]. Our results suggest that ROS production and the deactivation of AMPK by nano-alumina are early events in the pathogenesis of AD.

Conclusion

In conclusion, the present study postulates that nano-alumina are responsible for inducing toxic effects and decreasing cell viability by producing ROS *in vitro,* which can reach the brain and accumulate in exposed animals, inducing oxidative stress and neurodegeneration. Most importantly, our findings indicate that nano-alumina exposure make the CNS more vulnerable and accelerates multiple pathways, which may increase the chances of neurodegenerative disorders, such as AD.

Conflict of Interest

The authors declare no conflict of interest.

Acknowledgement

This research was supported by the Pioneer Research Center Program through the National Research Foundation of Korea funded by the Ministry of Science, ICT & Future Planning (2012-0009521).

Authors' contributions

This manuscript is designed and written by Dr. Shahid Ali Shah. Dr. Shah also performed all the western blots, immunofluorescence and ELISA experiments described here. Dr. Ashfaq Ahmad, Mr. Faheem Ullah and Dr. Faizul Amin conducted the cellular uptake experiments. The results are compiled by Mr. Gwang Ho Yoon. We are very thankful to Prof. Myeong OK Kim (PhD) for her kind attitude and giving us an opportunity as she is the corresponding author and holds all the responsibilities related to this manuscript.

References

1. B. Nowack and T. D. Bucheli, Occurrence, behavior and effects of nanoparticles in the environment, *Environ. Pollut.,* 2007, **150**, 5–22.
2. G. Oberdörster, V. Stone and K. Donaldson, Toxicology of nanoparticles: a historical perspective. *Nanotoxicology*, 2007, **1**, 2-25.

3. J. T. Kwon, D.S. Kim, et al, Inhaled fluorescent magnetic nanoparticles induced extramedullary hematopoiesis in the spleen of mice. *J. Occup. Health* 2009, **51**, 423-431.
4. M. Giovanni, J. Yue, L. Zhang, J. Xie, C. N. Ong and D. T. Leong, Pro-inflammatory responses of RAW264.7 macrophages when treated with ultralow concentrations of silver, titanium dioxide, and zinc oxide nanoparticles, *J. of Hazardous Materials*, 2015, **297**, 146–152.
5. M. Giovanni, C. Y.Tay, M. I. Setyawati, J. Xie, C.N. Ong, R. Fan, J. Yue, L. Zhang and D. T. Leong, Toxicity Profiling of Water Contextual Zinc Oxide, Silver, and Titanium Dioxide Nanoparticles in Human Oral and Gastrointestinal Cell Systems, *Environmental Toxicology*, DOI 10.1002/tox.
6. M. I. Setyawati, C.Y. Tay and D. T. Leong, Effect of zinc oxide nanomaterials-induced oxidative stress on the p53 Pathway, *Biomaterials*, 2013, **34**, 10133e10142.
7. R. Virginie, J. G. Hélène, C. Daniel, H. Catherine and D. Jean-François, Aluminum and silica in drinking water and the risk of Alzheimer's disease or cognitive decline: findings from 15-year follow-up of the PAQUID cohort, *Am. J. Epidemiol.,* 2009, **169**, 489–496.
8. Zhang et al, In vivo toxicity of nano-alumina on mice neurobehavioral profiles and the potential mechanisms, *Int. J. Immunopathol. Pharmacol.,* 2011, **24**, 23S-29S.
9. X. Li, Z. Hao, Z. Zhi-ren, L. Miao, et al, Glia activation induced by peripheral administration of aluminum oxide nanoparticles in rat brains, *Nanomedicine: Nanotechnology, Biology, and Medicine,* 2009, **5**, 473–479.
10. L. Chen, Z. Bei, T. Michal, Autophagy is involved in nanoalumina-induced cerebrovascular toxicity, *Nanomedicine: Nanotechnology, Biology, and Medicine*, 2013, **9**, 212–221.

11. J. A. Godoy, J. A. Rios, J. M. Zolezzi, B. Nady, C. I. Nibaldo, Signaling pathway cross talk in Alzheimer's disease, *Cell Communication and Signaling*, 2014, **12**:23.
12. M. Lin, M. F. Beal, Mitochondrial dysfunction and oxidative stress in neurodegenerative diseases, *Nature* 2006, **443**, 787–795.
13. M. Valko, D. Leibfritz, J. Moncol, et al, Free radicals and antioxidants in normal physiological functions and human disease, *Int. J. Biochem. Cell Biol.* 2007, **39**, 44–84.
14. A. Nunomura, G. Perry, G. Aliev, et al, Oxidative damage is the earliest event in Alzheimer disease, *J. Neuropathol. Exp. Neurol.,* 2001, **60**, 759–767.
15. M. F. Beal, Oxidative damage as an early marker of Alzheimer's disease and mild cognitive impairment, *Neurobiol. Aging*, 2005, **26**, 585–586.
16. M. A. Smith, X. Zhu, M. Tabaton, et al, Increased iron and free radical generation in preclinical Alzheimer disease and mild cognitive impairment, *J. Alzheimers Dis.,* 2010, **19**, 363–372.
17. M. Kawahara, Effects of aluminum on the nervous system and its possible link with neurodegenerative diseases, *J. Alzheimers Dis.,* 2005, **8**, 171–82.
18. M. Kawahara, M. Kato, Y. Kuroda, Effects of aluminum on the neurotoxicity of primary cultured neurons and on the aggregation of beta-amyloid protein, *Brain Res. Bull.,* 2001, **55**, 211–7.
19. W. A. Banks, A. J. Kastin, Aluminum induced neurotoxicity: alteration in membrane function at the blood brain barrier. *Neurosci. Biobehav. Rev.,* 1989, **13**, 47–53.
20. P. Zatta, M. Ibn-Lkhayat-Idrissi, P. Zambenedetti, M. Kilyen, T. Kiss, In vivo and in vitro effects of aluminum on the activity of mouse brain acetylcholinesterase, *Brain Res. Bull.,* 2002, **59**, 41–5.

21. B. Platt, G. Fiddler, G. Riedel, Z. Henderson, Aluminum toxicity in the rat brain: histochemical and immunocytochemical evidences, *Brain Res. Bull.,* 2001, **55**, 257–67.

22. C. Struys-Ponsar, A. Kerkhofs, A. Gauthier, M. Soffie, P. Van den Bosch de Aguilar, Effects of aluminum exposure on behavioural parameters in the rat. *Pharmacol. Biochem. Behav.,* 1997, **56**, 643–8.

23. A. Jyoti, P. Sethi and D. Sharma, Bacopa monniera prevents from aluminium neurotoxicity in the cerebral cortex of rat brain. *J. Ethnopharmacol.,* 2007, **111**, 56–62.

24. R. K. Gangwar, V. A. Dhumale, D. B. Kumari, U. T. Nakate, S. W. Gosavi, R. B. Sharma, et al., Conjugation of curcumin with PVP capped gold nanoparticles for improving bioavailability, *Mat. Sci. and Eng. C*, 2012, **32**, 2659–2663.

25. S. A. Shah, et al., Protection of the Developing Brain with Anthocyanins against Ethanol-Induced Oxidative Stress and Neurodegeneration, *Mol. Neurobiol.*, 2015, **51**, 1278-91.

26. A. S. Shahid, Y. L. Hae, A. B. Ray, J. Y. Dae and O. K. Myeong, Novel osmotin attenuates glutamate-induced synaptic dysfunction and neurodegeneration via the JNK/PI3K/Akt pathway in postnatal rat brain, *Cell Death and Disease,* 2014, **5**, 1-10.

27. R, Morris, Developments of a water-maze procedure for studying spatial learning in the rat. *J. Neurosci. Methods,* 1984, **11**, 47–60.

28. S. A. Shah, et al, Anthocyanins protect against ethanol-induced neuronal apoptosis via GABAB1 receptors intracellular signaling in prenatal rat hippocampal neurons, *Mol. Neurobio.,* 2013, **48**, 257–269.

29. B. Platt, G. Fiddler, G. Riedel and Z. Henderson, Aluminium toxicity in the rat brain: Histochemical and immunocytochemical evidence, *Brain Research Bull.,* 2001, **55**, 257–267.

30. S.A Shah, G. H. Yoon, H. Kim and M.O. Kim, Vitamin C Neuroprotection Against Dose-Dependent Glutamate-Induced Neurodegeneration in the Postnatal Brain, *Neurochem. Res.,* DOI 10.1007/s11064-015-1540-2.

31. J. F. Ge, C. C. Qi, J. P. Qiao. C. W. Wang and J. N. Zhou, Sex Differences in ICR Mice in the Morris Water Maze Task, *Physiol. Res.,* 2013, **62**, 107-117.

32. D. Julka, R. Sandhir, K. D. Gill, Altered cholinergic metabolism in rat CNS following aluminum exposure: implications on learning performance. *J. Neurochem.,* 1995, **65**, 2157–2164.

33. A. Kaur, K. Joshi, R. M. Walker, K. D. Gill, Neurofilament phosphorylation and disruption: a possible mechanism of chronic aluminium toxicity in Wistar rats, *Toxicology,* 2006, **219**, 1–10.

34. A. C. Miu, C. E. Andreescu, R. Vasiu and A. I. Olteanu, A behavioral and histological study of the effects of long-term exposure of adult rats to aluminum. *Intern. J. Neurosci.,* 2003, **113**, 1197–1211.

35. M. T. Colomina, J. L. Roig, D. J. Sánchez and J. L. Domingo, Influence of age on aluminum-induced neurobehavioral effects and morphological changes in rat brain. *Neurotoxicology,* 2002, **23**, 775-781.

36. T. P. Flaten, Aluminium as a risk factor in Alzheimer's disease, with emphasis on drinking water. *Brain Research Bull.,* 2001, **55**, 187–196.

37. Lee et al, Neurodegenerative Taupathies. *Annual Review of Neuroscience,* 2007, 1121-1159.

38. K. Iqbal, L. Fei, G. Cheng-Xin and I. Grundke-Iqbal, Tau in Alzheimer Disease and Related Tauopathies. *Curr. Alzheimer Res.,* 2010, **7**, 656–664.

39. D. Pratico, C. M. Clark, F. Liun, J. Rokach, V. Y. Lee and J. Q. Trojanowski, Increase of brain oxidative stress in mild cognitive impairment: a possible predictor of Alzheimer disease. *Arch. Neurol.,* 2002, **59**, 972–976.

40. E. Oesterling, N. Chopra, V. Gavalas, X. Arzuaga, E. J. Lim, R. Sultana, et al, Alumina nanoparticles induce expression of endothelial cell adhesion molecules. *Toxicol. Lett.,* 2008, **178**, 160–166.

41. M.I. Setyawati, C.Y. Tay, S.L. Chia, S.L. Goh, W. Fang , M.J. Neo, H.C. Chong, S.M. Tan, S.C.J. Loo, K.W. Ng, J.P. Xie, C.N. Ong, N.S. Tan, and D.T. Leong, Titanium dioxide nanomaterials cause endothelial cell leakiness by disrupting the hemophilic interaction of VE–cadherin, *Nature Communications*, **4**, 1673 DOI: 10.1038/ncomms2655.

42. I. M. Setyawati, C. Y. Tay, and D. T. Leong, Mechanistic Investigation of the Biological Effects of SiO 2 , TiO 2 , and ZnO Nanoparticles on Intestinal Cells, *Small***,** 2015, DOI: 10.1002/smll.201403232.

43. S. L. Chia, C. Y. Tay, M. I. Setyawati, and D. T. Leong, Biomimicry 3D Gastrointestinal Spheroid Platform for the Assessment of Toxicity and Inflammatory Effects of Zinc Oxide Nanoparticles, Small, 2014, DOI: 10.1002/smll.201401915.

44. C. Y. Tay, M. I. Setyawati, J. Xie, W.J. Parak, and D. T. Leong, Back to Basics: Exploiting the Innate Physico-chemical Characteristics of Nanomaterials for Biomedical Applications. *Adv. Funct. Mater.*, 2014, **24**, 5936–5955.

45. C. Exley, The pro-oxidant activity of aluminum. *Free Radic. Biol. Med.,* 2004a, **36**, 380–387.

46. M. G. Abubakar, A. Taylor and G. A. A. Ferns, Aluminium administration is associated with enhanced hepatic oxidant stress that may be offset by dietary vitamin E in the rat. *Int. J. Exp. Pathol.,* 2003, **84**, 49–54.

47. P. Sethi, A. Jyoti, R. Singh, E. Hussain and D. Sharma, Aluminium-induced electrophysiological, biochemical and cognitive modifications in the hippocampus of aging rats, *Neurotoxicology,* 2008, **29**, 1069-1079.

48. V. Kumar, A. Bal and K. D. Gill, Impairment of mitochondrial energy metabolism in different regions of rat brain following chronic exposure to aluminum, *Brain Res.,* 2008, **1232**, 94–103.

49. V. Kumar, A. Bal, K. D. Gill, Susceptibility of mitochondrial superoxide dismutase to aluminum induced oxidative damage. *Toxicology,* 2009, **255**, 117–123.

50. K. C. Cheng, D. S. Cahill, H. Kasai, S. Nishimura and L. A. Loeb, 8-Hydroxyguanine, an abundant form of oxidative DNA damage, causes G–T and A–C substitutions. *J. Biol. Chem.,* 1992, **267**, 166–172.

51. M. Dizdaroglu, P. Jaruga, M. Birincioglu and H. Rodriguez, Free radical-induced damage to DNA: mechanisms and measurement. *Free Radic. Biol. & Med.,* 2002, **32**, 1102–1115.

52. V. Kumar, A. Bal, K. D. Gill, Aluminium-induced oxidative DNA damage recognition and cell-cycle disruption in different regions of rat brain, *Toxicology*, 2009, **264**, 137–144.

53. R. Mailloux, J. Lemire and V. Appanna, Aluminum-induced mitochondrial dysfunction leads to lipid accumulation in human hepatocytes: a link to obesity. *Cell Physiol. Biochem.,* 2007, **20**, 627-638.

Figure legends

Figure 1. Shown are the images taken through TEM of various sizes and shaped of nano-alumina. The particle size of nano-alumina in water suspension was in 30-60 nm range.

Figure 2. The cellular uptake and toxic effects of nano-alumina *in vitro.* Shown are histograms for **(A)** cell viability, cytotoxicity and caspase-3/7 activation in SH-SY5Y cells **(B)** and ROS quantification in SH-SY5Y and HT22 cells after nano-alumina treatment. The cells were cultured in 96-well plates, and then treated with nano alumina for the indicated time. ApoTox-GloTM Triplex and ROS detection assays were performed as described in the materials and methods section. **(C, D)** The uptake experiment was performed with mouse bEnd3 and human neuroblastoma SH-SY5Y cells. Shown are the immunoflourescence images of **(C)** mouse bEnd3 cells with or without treatment of rhodamine 123-conjugated nano-alumina (red) and **(D)** in human neuroblastoma SH-SY5Y cells of treated or untreated coumarin-6-conjugated nano-alumina (green) for 24 hr. Representation of the immunofluorescence images **(E)** Morin (green), DAPI (blue) **(F)** 8-OxoG (green), DAPI (blue) staining in HT22 cells after exposure to nano-alumina for 12 hours. Details are in the methods section. All the experimental results *in vitro* were repeated in triplicate and represent the mean ± SEM of three separate experiments. Significant differences were determined using one-way analysis of variance (ANOVA) followed by Student's t-test. Significance = $^{*, **, ***}P < 0.05, 0.01, 0.001$.

Figure 3. Nano-alumina caused aluminium abundance and oxidative stress in the brain of female ICR mice. Representative images with integrated density histograms of **(A)** Morin (green) **(B)** 8-OxoG (red), DAPI (blue) staining in the hippocampal and cortical regions after nano-alumina administration to female ICR mice. These images shows green fluorescence (Morin staining) and red fluorescence (8-oxoG staining) in nano-alumina treated mice and almost no signals in the untreated mice brain sections (n=5 mice/group). Significant differences were determined using one-way analysis of variance (ANOVA) followed by Student's t-test. Significance = $^{***}P < 0.001$.

Figure 4. Nano-alumina impaired the behaviour and induced toxic Aβ production in the mice brain. The Morris water maze (MWM) test was performed to analyse the toxic effect of nano-alumina treatment on spatial memory in female ICR mice. Shown is the escape latency time (**A**) before treatment (**B**) and after treatment during the training period (submerged platform) of the MWM test. The arrow indicates time of treatment. (**C**) Shown is the time spent in the target quadrant during the MWM probe test (platform removed), expressed as a percent of alternation. Data represent the mean ± SEM (n=5/group). (**D**) Presented are the immunoblots along with respective densitometry histograms of APP, sAPP-α, BACE1 and Aβ of treated and untreated female ICR brain homogenates. Mice were treated with nano-alumina for three weeks and their brains were separated. Sigma Gel software was used for the quantification of the protein bands. β-actin was used as a loading control. The density values are expressed in arbitrary units (A.U) as the means ± SEM for the respective indicated proteins (n=5 mice/group). (**E**) Shown is the ELISA assay result histogram of soluble $A\beta_{1\text{-}42}$ (pg/ml) in the brain homogenates of 10 week-old nano-alumina treated and untreated ICR female mice. Significance; $^{**, ***}P< 0.01, 0.001$.

Figure 5. Nano-alumina induced toxic Aβ aggregation and reduced pre-and post-synapse related proteins expressions in the female mice brain. Shown are fluorescence images of hippocampus and cortex of 10 week-old nano-alumina treated and untreated ICR female mice indicating the localization of Aβ aggregation and Aβ plaques after **(A)** Aβ (6E10) and **(B)** Thioflavin S (green) staining along with PI counterstaining. Immunoblots and integrated densitometry histograms showing the expression of (**C**) phosphorylated tau, total tau protein, (**D**) pre-and post-synapse related proteins, including Synaptophysin and PSD 95 in the hippocampus and cortex of nano-alumina treated and untreated mouse brain. Sigma Gel and image J software was used for the quantification of the protein bands and immunofluorescence images, respectively. β-actin was used as a house keeping gene. Significance; $^{**, ***}P< 0.05, 0.01$

Figure 6. Nano-alumina reduced the expression and activity of AMPK in the female mice brain. Immunoblots and integrated densitometry histograms of (**A**) p-AMPK and total AMPK showing the expression (**B**) AMPK activity histogram in the hippocampus and cortex of nano-alumina treated and untreated mice brain. (**C**) Immunofluorescence images of p-AMPK (red), DAPI (blue) and integrated density histogram of treated and untreated female ICR brain homogenates. Details are given in the material and methods section. Significance; $^{**, ***}P< 0.01, 0.001$.

Figure 7. Nano-alumina upregulated the expression of different apoptotic markers and induced neurodegeneration in the mice brain. The representative immunoblots of various (**A**) apoptotic markers, including cleaved caspase-3 and cleaved PARP-1, in the nano-alumina treated and control mice. The histograms containing their density details are also given here. **(B)** Representation of the green colour Fluoro Jade B (FJB) positive neuronal cells counterstained with DAPI (blue) in the cortical and hippocampal CA1, CA3, DG regions of the female ICR

mice brain after exposing to nano-alumina for three weeks. FJB details were discussed in the materials and methods section. These images are representative of the staining obtained in the sections (n=5 animals/group). Significance = $^{**, ***}P < 0.01, 0.001$.